Intrinsically Stretchable, Semi-transparent Organic Photovoltaics with High Efficiency and Mechanical Robustness via Full Solution Process

Jiaming Huang[1], Zhen Lu[1], Jiaqi He[1,2], Hong Hu[3], Qiong Liang[1], Kuan Liu[1], Zhiwei Ren[1], Yaokang Zhang[2], Hongyu Yu[2], Zijian Zheng[3] and Gang Li[1]*

J. Huang, Z. Lu, J. He, Q. Liang, Dr. K. Liu, Dr. Z. Ren, and Prof. G. Li

Department of Electronic and Information Engineering, Research Institute for Smart Energy (RISE), The Hong Kong Polytechnic University, Hung Hom, Kowloon, Hong Kong, China.

The Hong Kong Polytechnic University Shenzhen Research Institute, Shenzhen 518057, China.

E-mail: gang.w.li@polyu.edu.hk

J. He, Prof. H. Yu

School of Microelectronics, Southern University of Science and Technology, Shenzhen, China

Dr. H. Hu, Dr. Y. Zhang, Prof. Z. Zheng

Laboratory for Advanced Interfacial Materials and Devices, Institute of Textiles and Clothing, The Hong Kong Polytechnic University, Hung Hom, Kowloon, Hong Kong, China.

Methods

Materials

The silver nanowires (AgNWs) dispersion in isopropyl alcohol (IPA) (D: 30 nm, L: 30 μm, 10 mg/ml) is purchased from Beijing Deke Daojin Science And Technology Co., Ltd. PM6, BTP-eC9, PY-IT, N2200 were purchased from Solarmer Materials Inc, Beijing. TPU Elastollan 685 A was purchased from Basf. Al-doped Zinc oxide, chlorobenzene, chloroform (CF), N,N-dimethylformamide (DMF), 1,8-diiodioctane (DIO), and 1-chloronaphthalene (CN) were purchased by Sigma-Aldrich. Poly(3,4-ethylenedioxythiophene): poly(styrenesulfonate) (PVP AI4083) was purchased from Heraeus Deutschland GmbH & Co. KG. Patterned ITO/glass substrates were purchased from Huananxiangcheng Ltd. All materials and solvents were used as received without further purification.

Device Fabrication

For the device based on AgNWs@TPU, AgNWs were diluted into IPA and were put into a sonication bath for 5-10 min until good dispersion. The AgNWs were spin-coated onto a pre-cleaned glass with 2000 rpm, then thermal annealing at 200 °C for 5 min and 150 °C for 15 min. The pattern was achieved by polyimide tape. The AgNWs film was then soaked in deionized water (DI-water) to remove the surfactant and dry at 110 °C for 10 min. Then the TPU (200 mg/ml in DMF) was spin-coated on AgNWs at 1000 rpm for 1 min and dry at 80 °C for 5 h. Then the TPU@AgNWs were prepared after peel-off from the glass substrate. The silver paste was painted at the edge of AgNWs for contact.

Before spin-coating PEDOT:PSS, the AgNWs@TPU were UV-ozone treated for 5 min. PEDOT:PSS was spin-coated with 3000 rpm for 30 s and then annealed at 110 °C for 15 min. Then the samples were moved into the glovebox. Afterwards, for the active layer, the PM6:BTP-eC9 (22 mg/ml in CB, D:A = 1:1.2, 0.5% DIO, 2000 rpm/30s), PM6:PY-IT (14 mg/ml in CF, D:A = 1:1, 1% CN, 2000 rpm/30s), and PBDB-T:N2200 (10 mg/ml in CB, D:A = 2:1, 1% DIO, 2000 rpm) were deposited onto the PEDOT:PSS films and annealing at 100°C for 10 min. Then, AZO dispersion (0.8% wt in IPA) was spin-coated onto active layers at 2000 rpm for 30 s. After annealing at 60°C for 8 min, the AgNWs (5 mg/ml) were spin-coated onto AZO at 1000 rpm for 30 s and annealed at 100 °C for 10 min. For the AAA back electrode, another AZO (2.5% wt in IPA) was spin-coated onto AgNWs at 1000 rpm for 30 s. The pattern was achieved by PDMS. The silver paste was painted at the edge of AgNWs for contact. For the devices based on Ag electrode, Ag (100 nm) was evaporated through a shadow mask. The effective area of the device is 0.04 cm^2.

For the device based on ITO/glass, the patterned ITO was sonically cleaned in detergent aqueous solution, DI-water, acetone, and IPA for 40 min subsequently. After UV-Ozone treatment for 20 min, the PEDOT:PSS was spin-coated. The following procedures are the same as the details above. For OLED devices, the active layer material is spiro co-polymer with a concentration of 8 mg/ml in toluene.[1] Then spin-coating with 2000 rpm for 40 s followed by thermal annealing at 100°C for 10 min. Other steps are similar to *is*-OPV.

Simulation

1 Details of the adhesion failure under tensile strain

The model was performed in the commercial software Abaqus with the dynamic/explicit solver. All the materials were assumed isotropic and linearly elastic. To ensure the model is a quasi-static process, the total kinetic energy was strictly constrained to only 1% of the total strain energy by tuning the time period. When the two contact surfaces separated from each other, they experienced attractive traction, which increased linearly to the maximum of $\sigma = \sigma_m$ at the separation of $\delta = \delta_m$. Afterward, the traction decayed linearly and finally vanished. The failure degree of the CZM (D) can define the detachment of the NWs on the substrate. When the CZM started to decay (*i.e.*, $\delta = \delta_m$) D was equal to 0. As D increased to unity with the increase of δ, no attractive attraction was applied to the interface, indicating the complete detachment of the NWs. The area underneath the traction-separation curve was defined as the toughness (or namely, interfacial binding energy) of the interface (Γ). To reveal the geometrical confinement effect of the upper AZO in preventing the detachment of nanowires, we assumed that there was also an interface between the upper AZO and underlying AZO ETL. Differing from the nanowire-AZO interface (interface 1), the material at the two sides of this interface (interface 2) was the same (AZO). Regarding neglectable material mismatch, interface 2 was assumed to be much stronger than interface 1 (*i.e.*, Γ_2 is much larger than Γ_1). With these definitions, a displacement boundary condition was applied on the plane of the right-hand side of the substrate to stretch the part. The right-hand side plane is symmetrical, while the back- and front sides were periodic boundaries.[2]

The parameters used in our model are included in the following table.

Item	Value
Young's modulus of nanowires, E_{NW} /GPa	120
Young's modulus of AZO, E_{AZO} /GPa	80
The radius of nanowires, R_{NW} /nm	15
The thickness of upper AZO coverage film t_{AZO}/ nm (only in model b)	25
δ_m for CZM / nm	1.5
σ_m for CZM / GPa	0.2
Toughness of interface 1, Γ_1 / J/m^2	0.05
Toughness of interface 2, Γ_2 / J/m^2	0.5

2 Details of the electric potential simulation by COMSOL Multiphysics

The COMSOL Multiphysics commercial software package is used for the electrical characterization of the AAA STE system in this study. The program simulates electrical components (conductivity and permittivity) and devices used in electrostatic applications, particularly in terms of the effects of other physical properties.

The three-dimensional numerical model used in this study incorporates an AC/DC module (Electric Currents, Stationary). The width, length, and height of the AZO substrate are 1 μm, 1 μm, and 50 nm, respectively. The origin of the coordinate is in the corner of the AZO substrate. Two Ag nanowires cross electrodes (radius: 20 nm) with a central overlap are set on the AZO surface. The conductivity of Ag nanowires and AZO are 10^4 S/cm and 10^{-3} S/cm, respectively. The boundary conditions used are meant to represent a connection to a DC source of voltage. The bottom of the AZO substrate is grounded, representing a zero potential point, and the upper surfaces of Ag nanowires are connected to a constant voltage source of 8×10^{-5} V, using the Terminal boundary condition.

To improve the electric potential distribution of impedance measurement, a series of additional AZO coverage with different thicknesses have been proposed in this study. The AZO coverage is set to partially surround or fully surround the cross electrodes and fill the gap between the two Ag nanowires, and the electrical properties are the same as the AZO substrate. The mesh is set to Free Tetrahedral and the predefined accuracy is set to Extra Fine.

After the computing, the 3D electric potential mapping can be extracted from the convergent model. The 1D potential distribution in the Ag nanowires/AZO substrate interface along the vertical and lateral directions is plotted and the integrated intensity of the whole interface can be calculated by the Boundary Probe.

Characterization

The *J-V* curves were measured in the glovebox with a Keithley 2400 unit under 1 sun, AM 1.5G spectra (100 mW·cm^{-2}) from a solar simulator (Enli Tech. Co., Ltd., Taiwan). The light intensity was calibrated with a 20 mm × 20 mm monocrystalline silicon reference cell with a KG5 filter (Enli Tech. Co., Ltd., Taiwan). The EQE spectra were measured by QE-R3-011 (Enli Tech. Co., Ltd., Taiwan). The light intensity at each wavelength was calibrated with a standard single-crystal Si photovoltaic cell. The OPV device used for the mechanical stability test is the translucent device with the bottom illumination under AM 1.5G (100 mW·cm^{-2}). The mechanical stability (bending, twisting, and stretching) was performed by a linear reciprocating motor in the glovebox without encapsulation. The sheet resistance was conducted by four-terminal measurement. Transmittance and absorption were measured by Varian Cary® 300 UV-Vis spectrophotometers (Agilent Technologies). Conductive AFM was conducted by a Bruker Dimension ICON. Resistance variation is conducted by an electrochemical workstation (AUTOLAB, PGSTAT 302N).

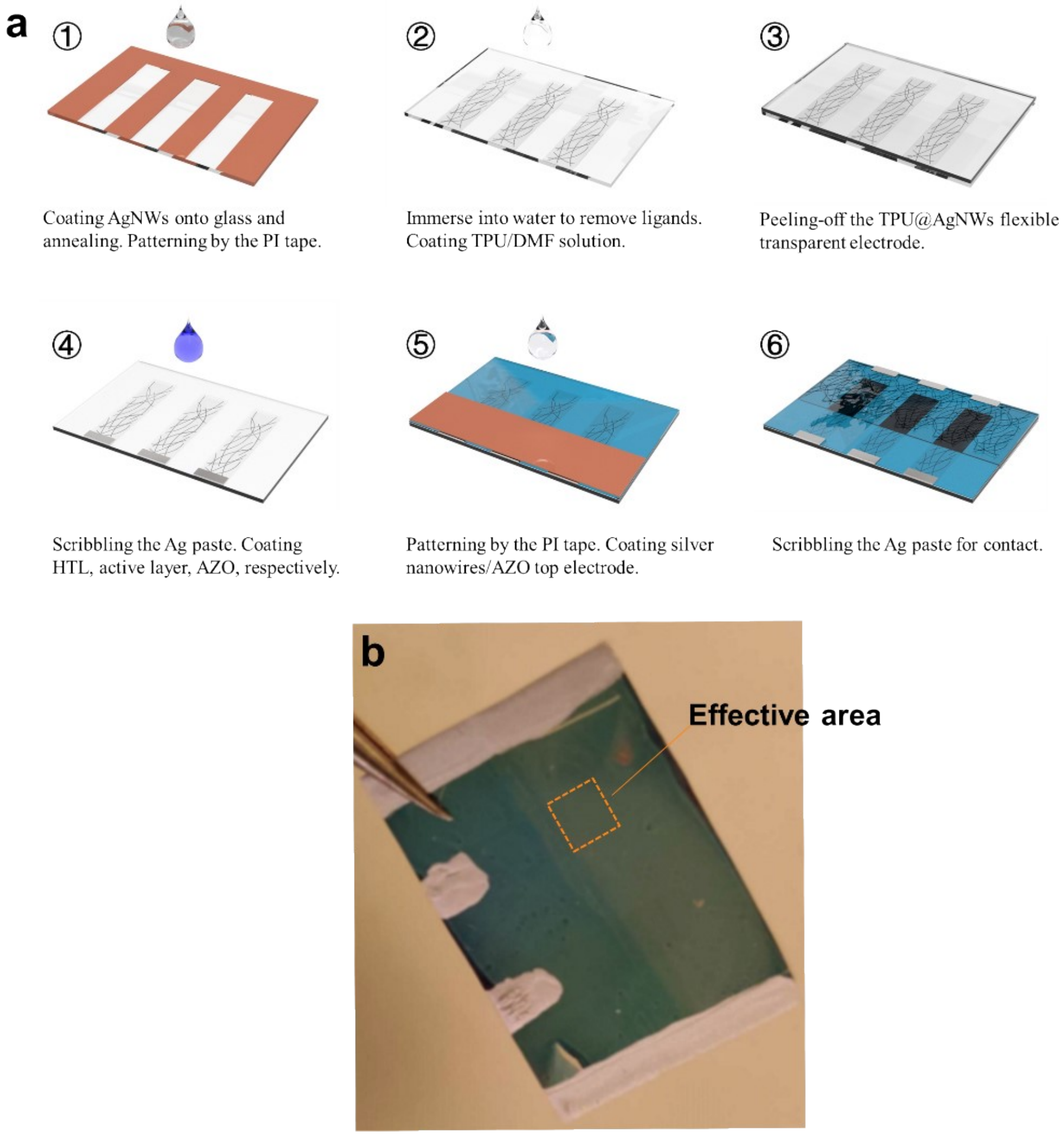

Figure S1 a) Fabrication of *is*-OPV by full solution process; b) Photograph of the device with the marked effective area.

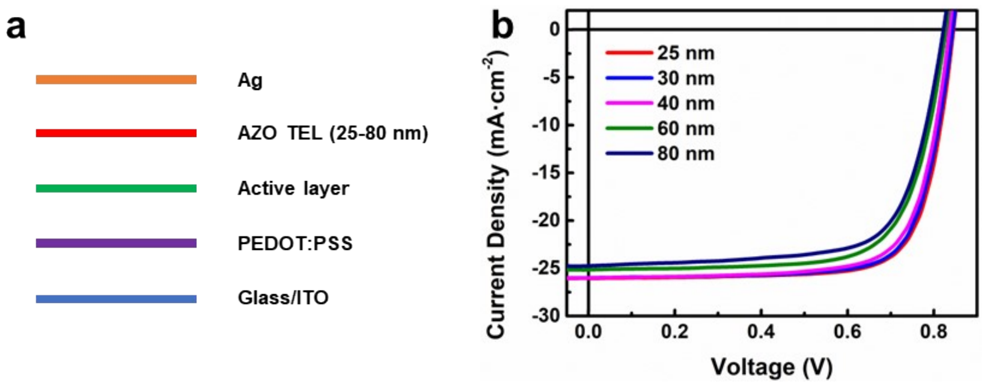

Figure S2 a) Device configurations and b) *J-V* curves of the AZO-based ETL

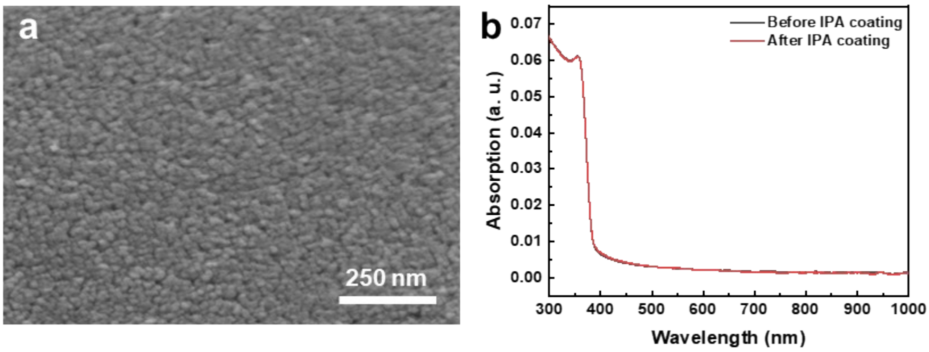

Figure S3 a) SEM image of the AZO ETL after coating IPA; b) Absorption spectra of AZO fims before and after IPA coating.

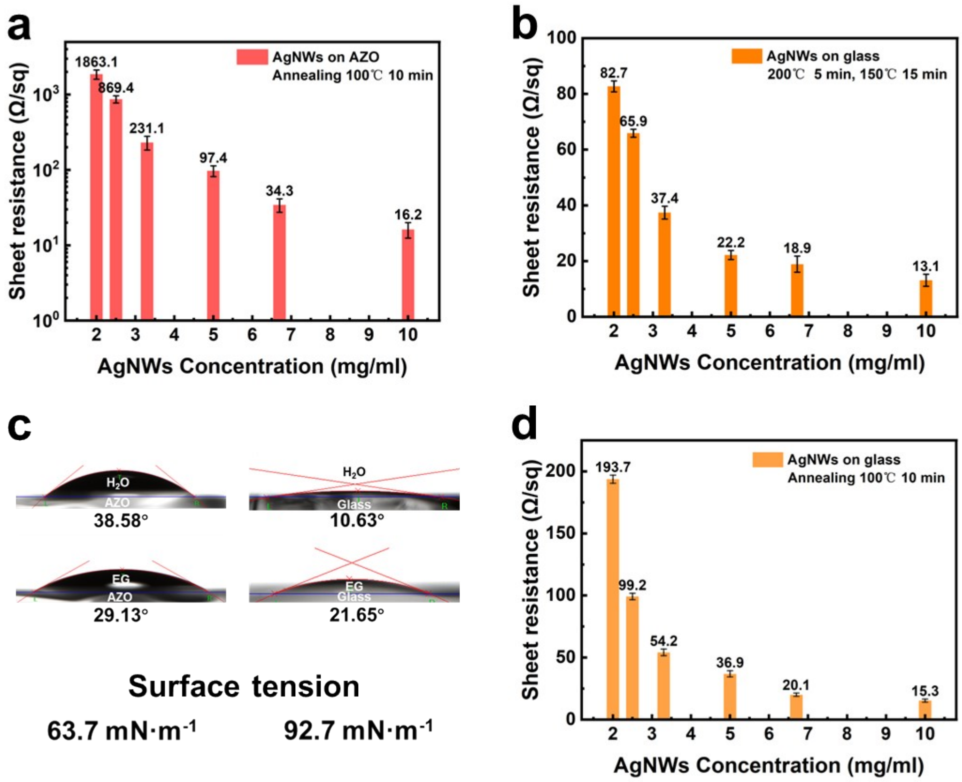

Figure S4 Sheet resistance of the AgNWs networks coating on a) AZO with annealing condition (100℃/10 min), b) neat glass with annealing condition (200℃/5 min and 150℃/15 min), d) neat glass with annealing condition (100℃/10 min); c) contact angle of H_2O and ethylene glycol on AZO and neat glass and their surface potential.

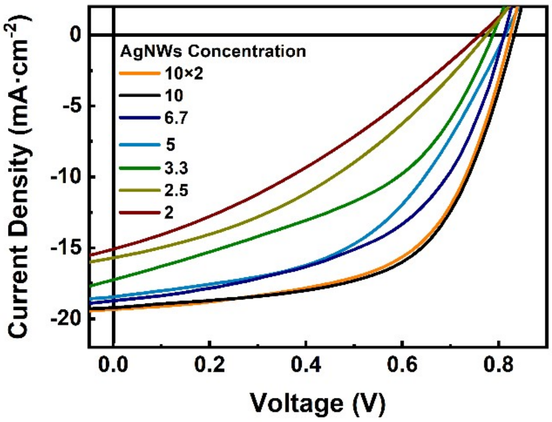

Figure S5 *J-V* curves of the OPV devices based on bare AgNWs back electrode with different AgNWs concentrations

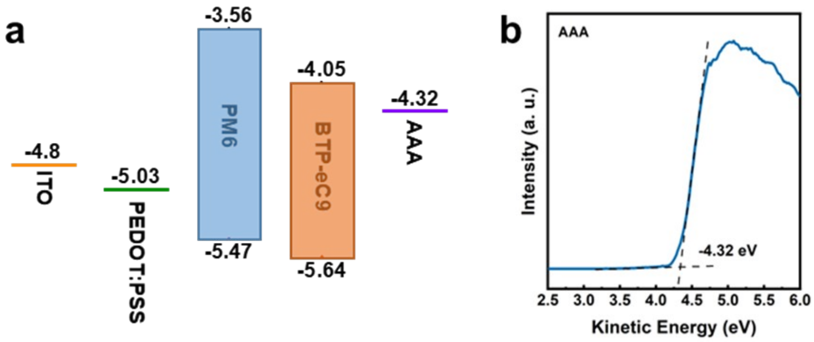

Figure S6 a) Energy diagram of the device; b) UPS spectra of the AAA electrode.

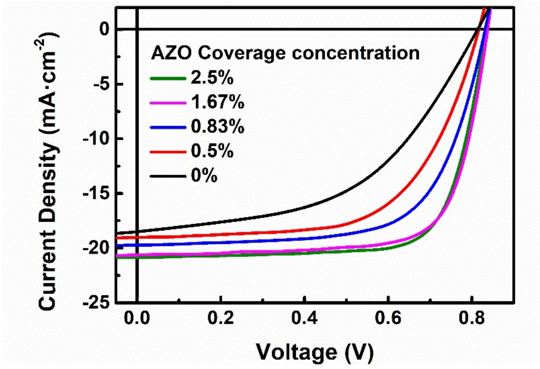

Figure S7 *J-V* curves of the devices based on AAA STE based on AZO coverage with different concentrations.

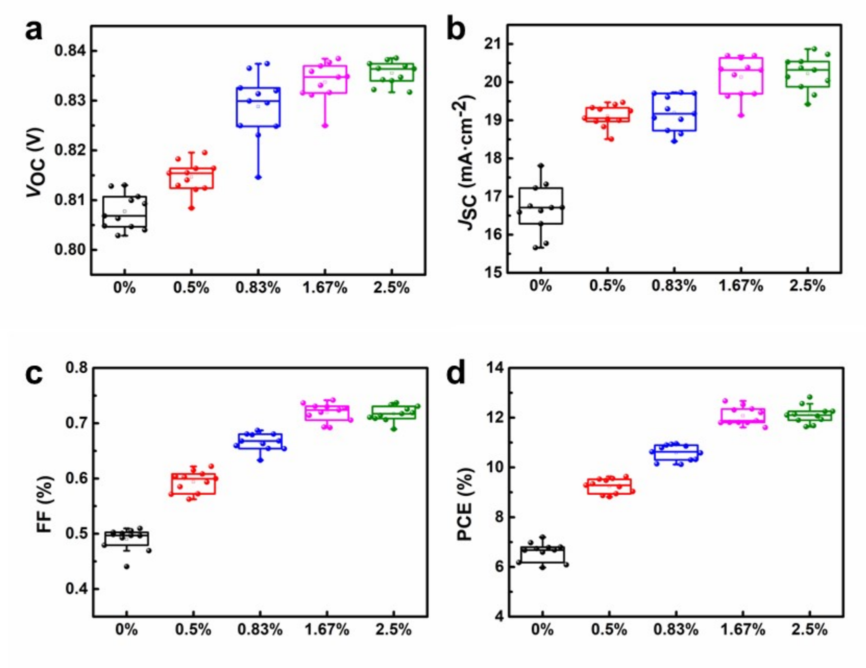

Figure S8 Device performance. (a) V_{OC}, (b) J_{SC}, and (c) FF and (d) PCE parameters comparisons of the devices that deposited with different AZO concentrations with 1000 rpm.

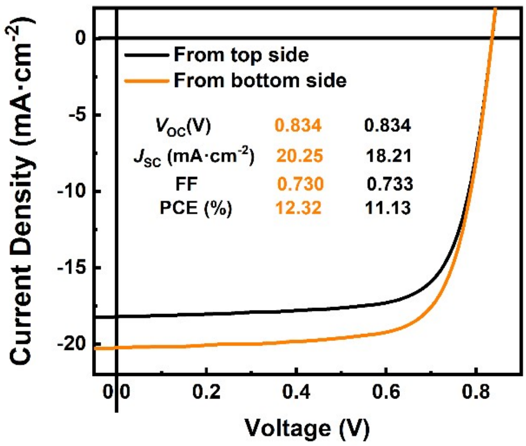

Figure S9 *J-V* curves of the device with the structure of ITO/PEDOT:PSS/PM6:BTP-eC9/AAA when illuminated from the top and the bottom side under simulated AM1.5G, respectively.

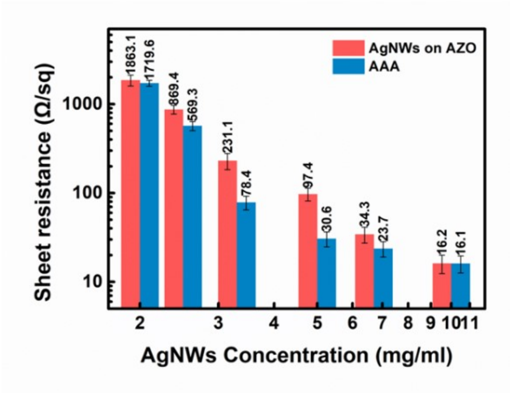

Figure S10 Sheet resistance of AgNWs/AZO and AAA electrodes with different AgNWs concentrations (AZO coverage with a concentration of 2.5%)

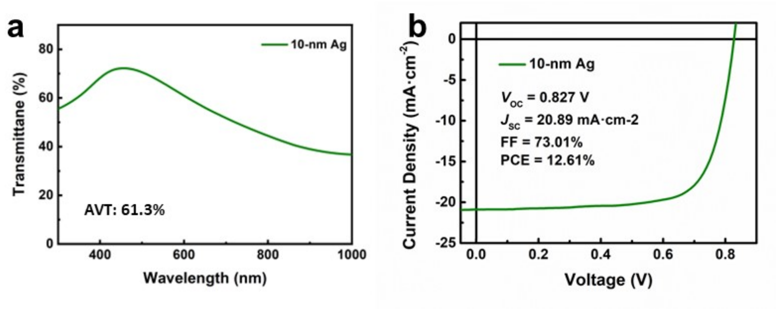

Figure S11 a) Optical transmittance of the 10-nm Ag electrode fabricated by thermal evaporation; b) *J*-*V* curves of the semi-transparent OPV devices based on 10-nm Ag as the back electrode

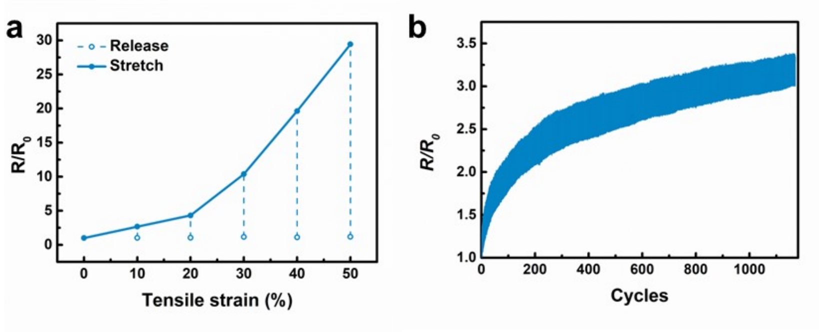

Figure S12 a) Sheet resistance variation of AAA STE under different tensile strains; b) Long-term mechanical stability under continuous bending with a tensile strain of 20%.

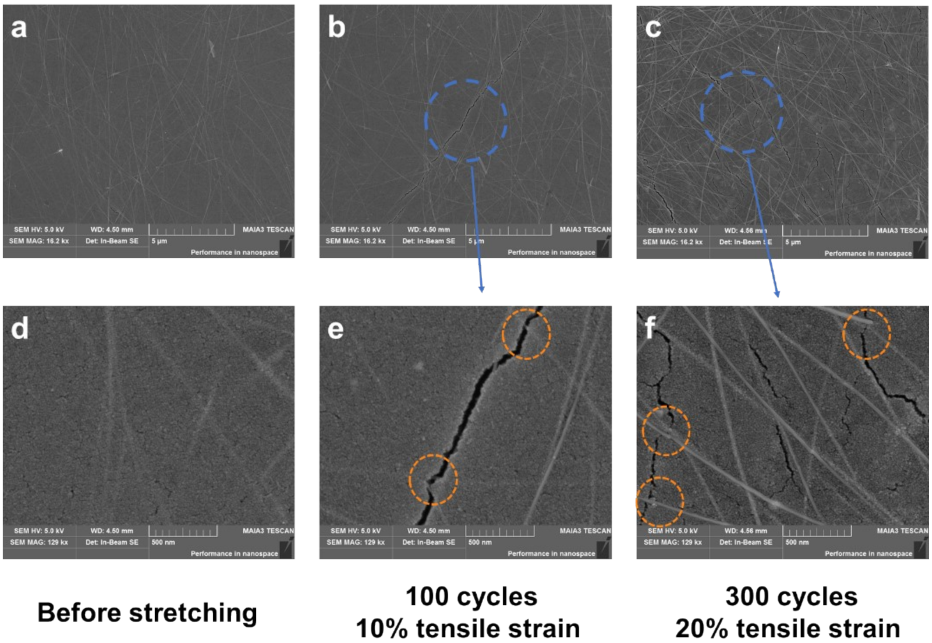

Figure S13 SEM micrographs of AAA electrode before and after stretch-release cycles. The AgNWs marked by organic circles is not broken after continuous stretch-release cycles.

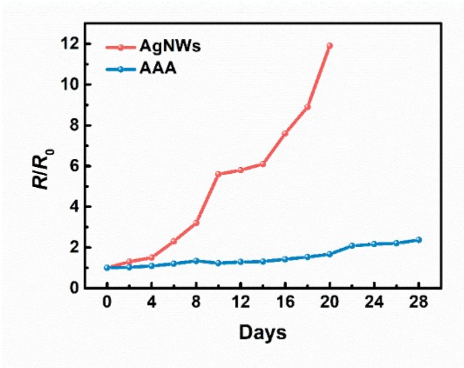

Figure S14 Air ambient stability of the bare AgNWs and AAA composited STE

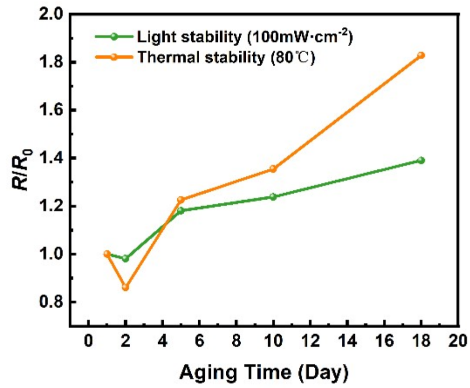

Figure S15 Light stability and thermal stability of the AAA electrode in ambient conditions.

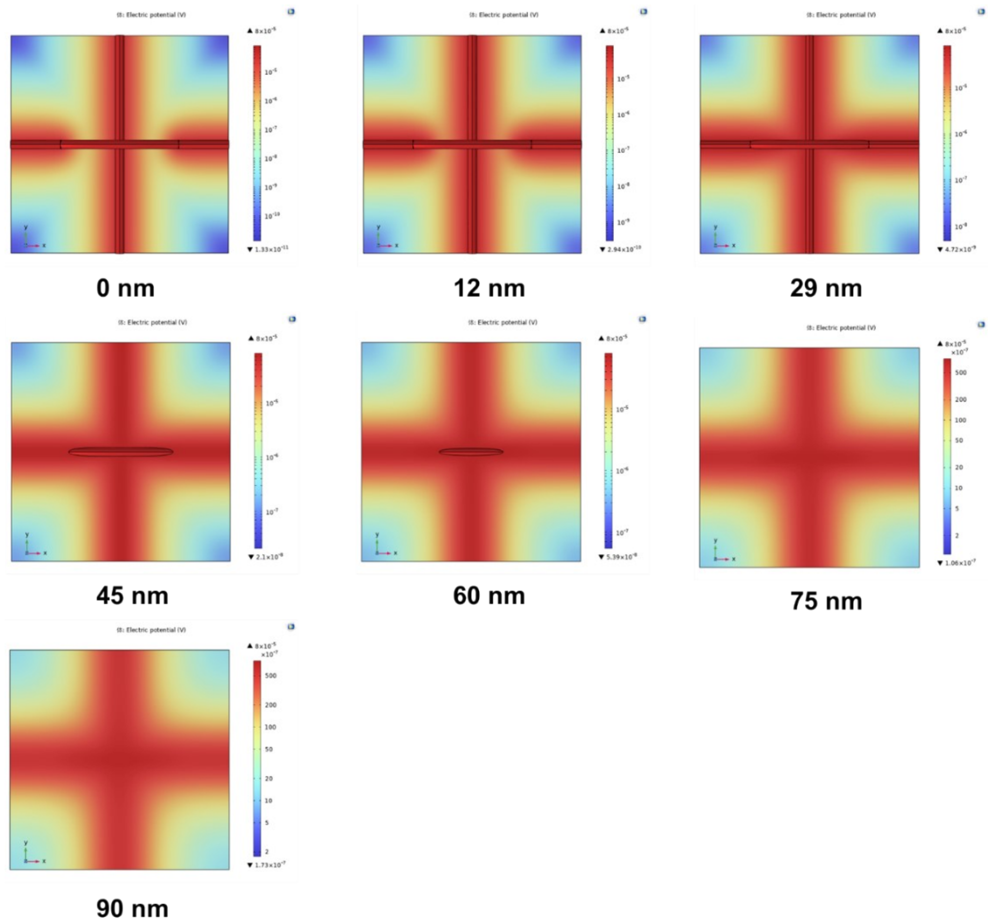

Figure S16 Top view of the COMSOL simulation of the AAA STE with different thicknesses of AZO coverage

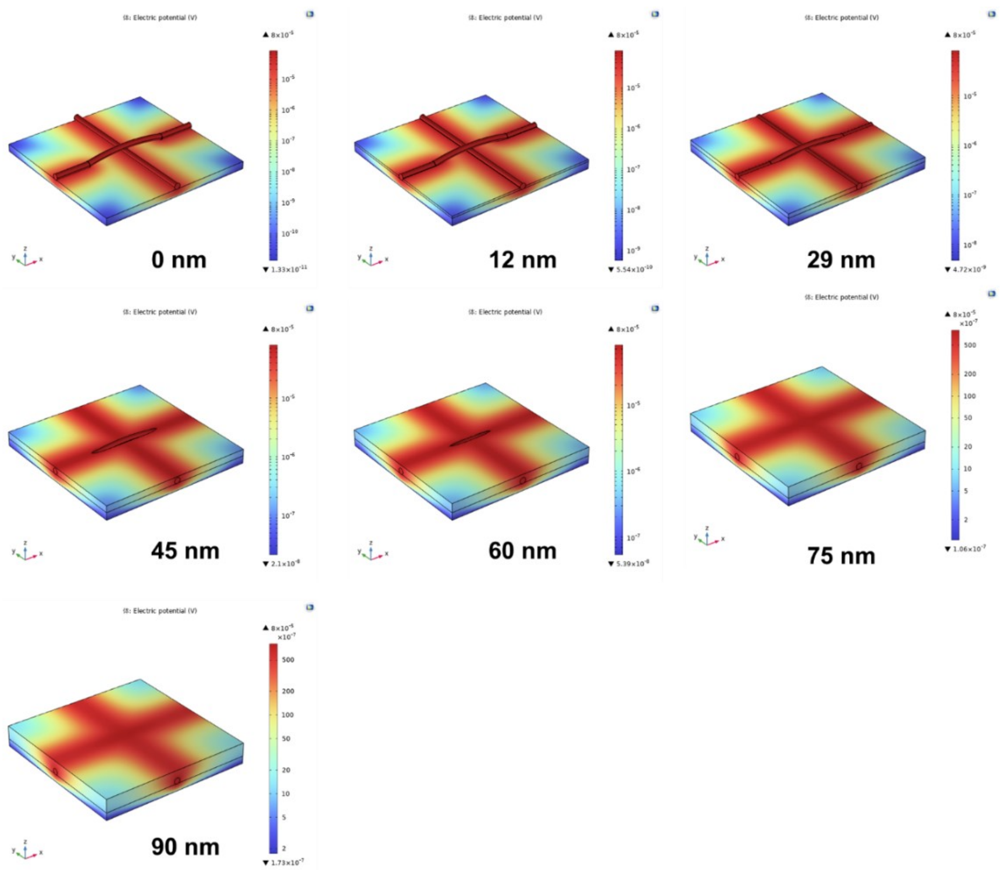

Figure S17 Perspective view of the COMSOL simulation of the AAA STE with different thickness of AZO coverage

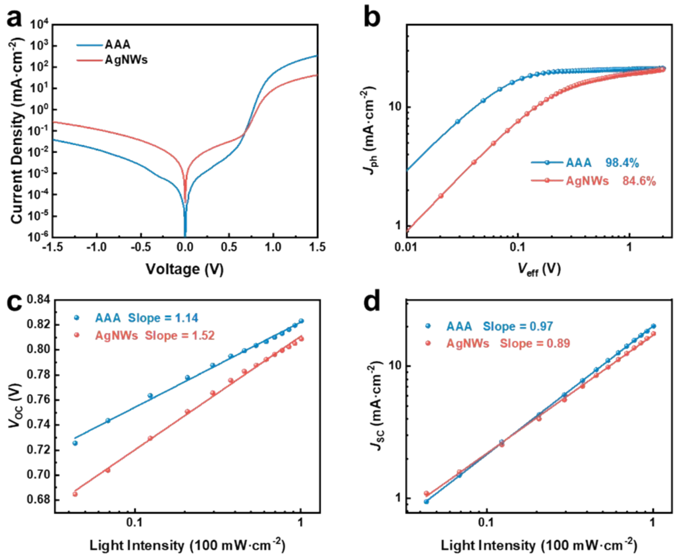

Figure S18 Photophysical processes of the devices based on AAA and AgNWs back STE. a) *J-V* curves under dark conditions; b) Photocurrent *versus* effective voltage; c) Light intensity-dependent V_{OC} and d) Light intensity-dependent J_{SC}.

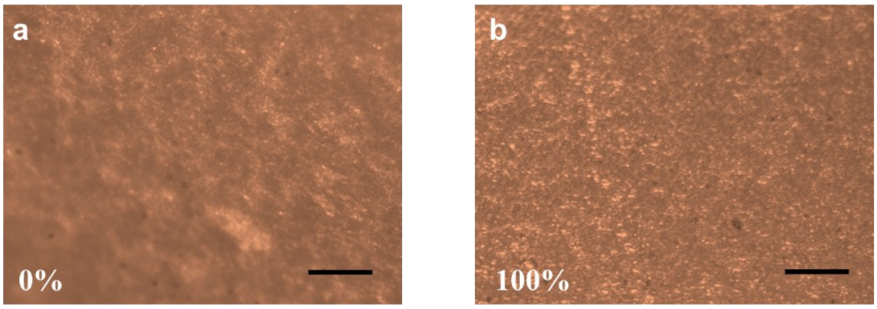

Figure S19 Images of TPU @AgNWs in microscope under a) 0% tensile strain and b) 100% tensile strain (Scale bar: 150 um)

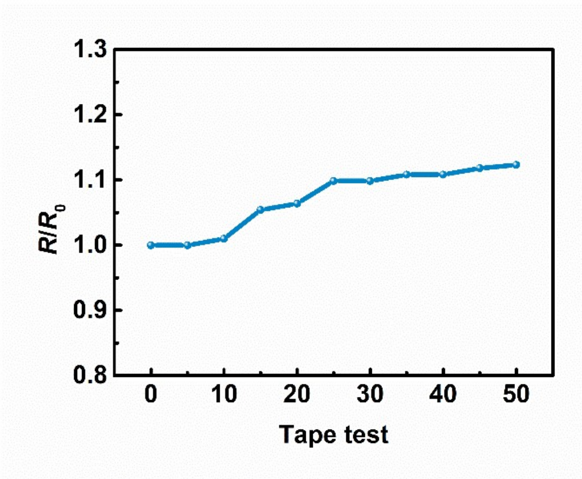

Figure S20 Sheet resistance variation of the TPU@AgNWs after tape test

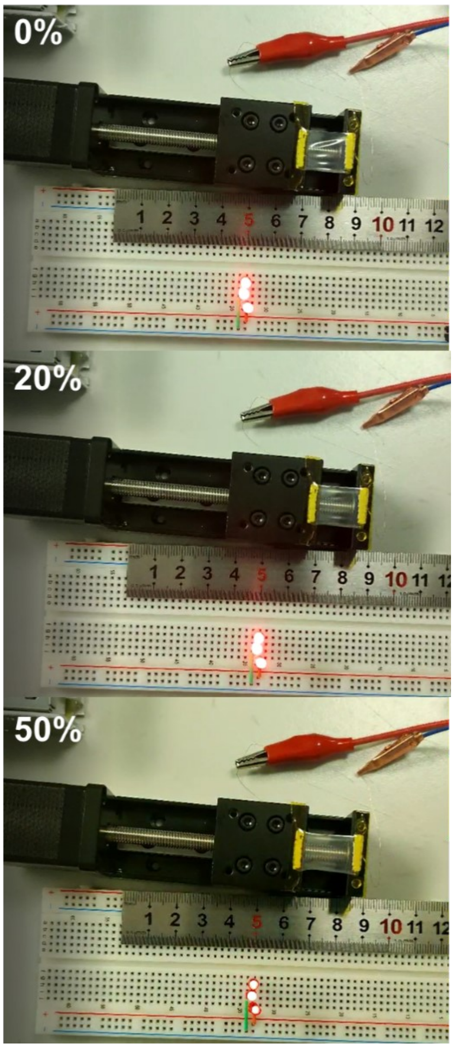

Figure S21 Stretched TPU@AgNWs serve as the interconnect to drive commercial LED

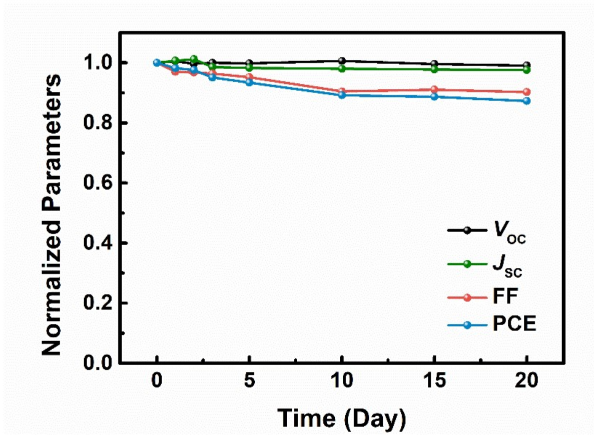

Figure S22 The shelf lifetime of the *is*-OPV device

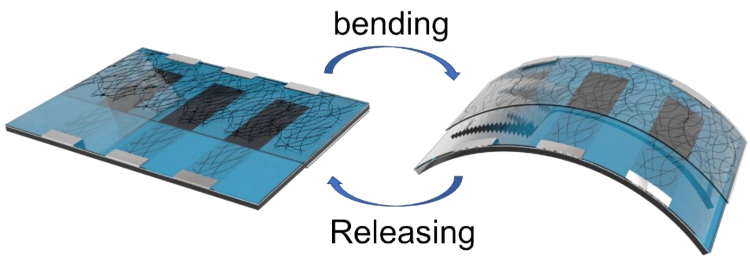

Figure S23 The schematic diagram of the device bending direction.

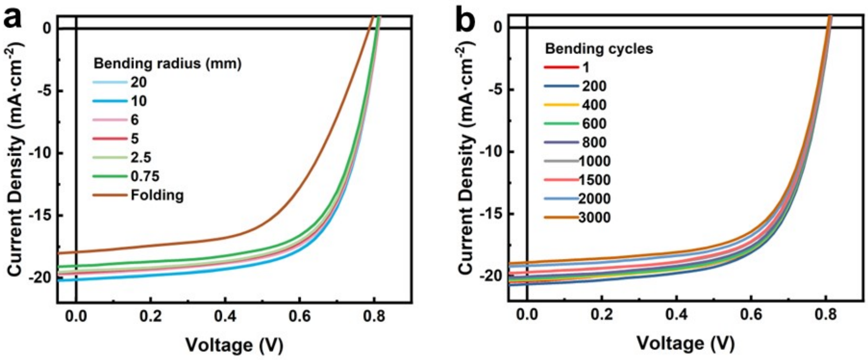

Figure S24 The representative *J-V* curves of the devices based on PM6:BTP-eC9 a) after 200 cycles of continuous bending with different curvature radii, b) 3000 cyclic bending-flatting processes with a 1.5 mm curvature radius.

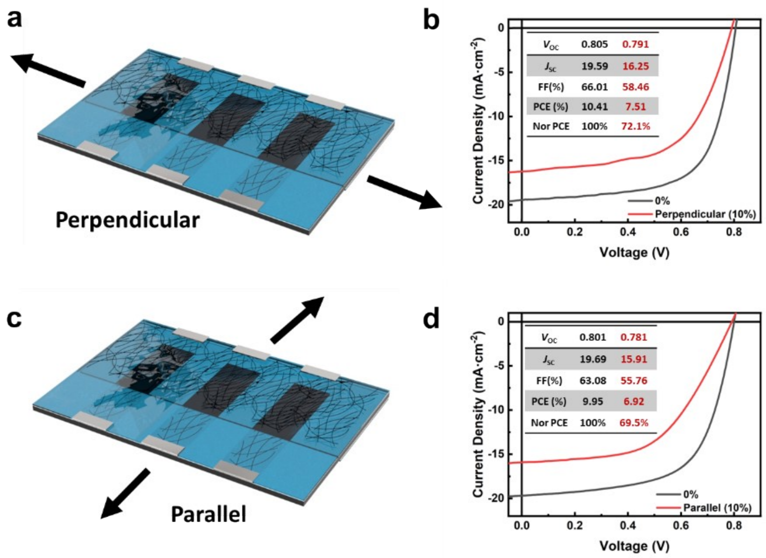

Figure S25 Schematic diagrams of the stretching direction. a) perpendicular and b) parallel directions; The *J*-*V* curves of the devices based on PM6:BTP-eC9 under tensile strain with c) perpendicular and d) parallel directions.

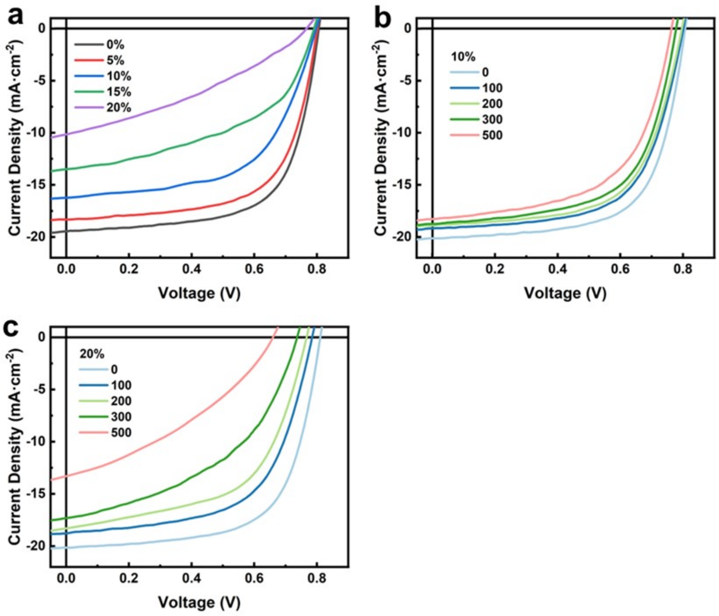

Figure S26 The representative *J-V* curves of the devices based on PM6:BTP-eC9 a) under different tensile strains, b) after continuous stretch-release cycles with 10% tensile strain, c) after continuous stretch-release cycles with 20% tensile strain.

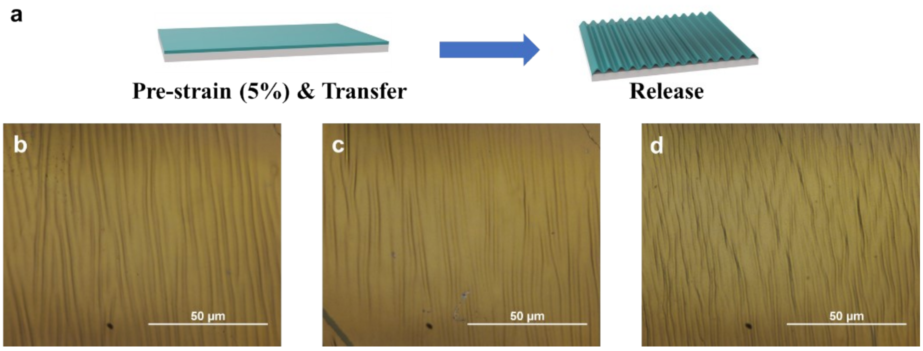

Figure S27 a) The process of the buckling methods; Surface buckling of the active layers fabricated on PDMS b) PM6:BTP-eC9, c) PM6: PY-IT, d) PBDB-T:N2200

The organic active layers were fabricated on the elastomer PDMS by transfer. A small (<5%) compression was then applied to the PDMS-based samples and there would be buckled with a specific wavelength. Then the elastic modulus of the target films was calculated from the following equations[3, 4]:

$$E_f = 3E_s\left(\frac{1 - v_f^2}{1 - v_s^2}\right)\left(\frac{\lambda}{2\pi d_f}\right)^3$$

Where the E_f is the elastic modulus of target films, E_s is the elastic modulus of substrate PDMS (1.8 MPa), v_f is the Poisson ratios of the target films (0.35), v_s is the Poisson ratios of the substrate (0.5), λ is the wavelength of the buckling and d_f is the thickness of films.

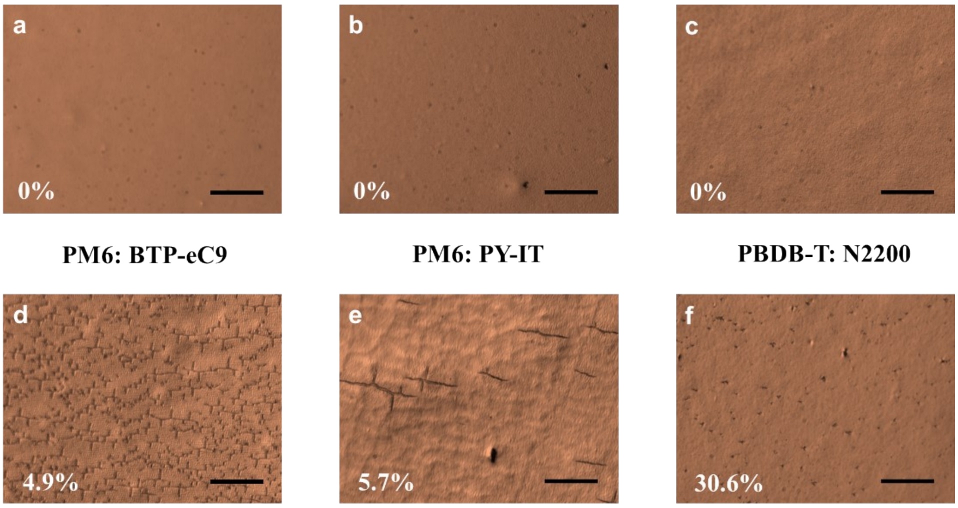

Figure S28 COS of the active layers (Scale bar: 150 um)

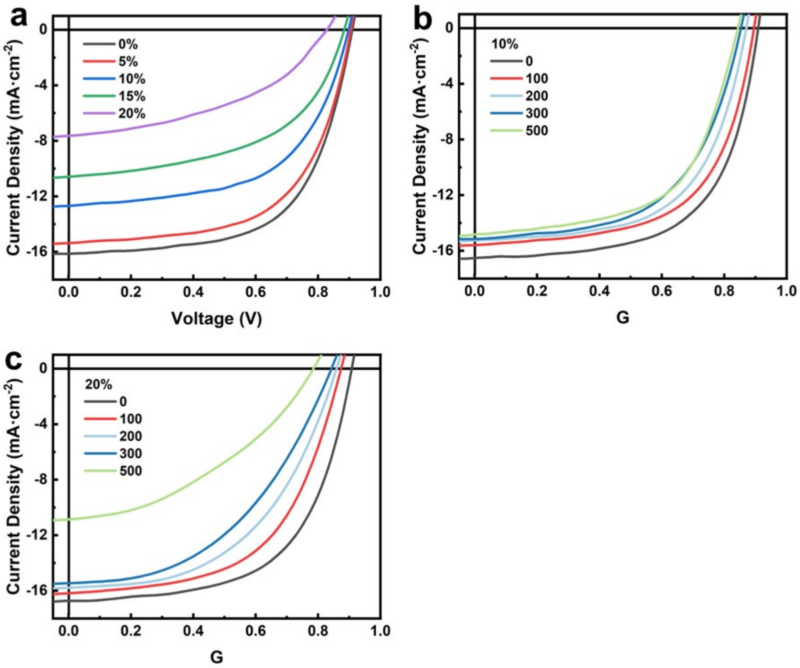

Figure S29 The representative *J-V* curves of the devices based on PM6:PY-IT a) under different tensile strains, b) after continuous stretch-release cycles with 10% tensile strain, c) after continuous stretch-release cycles with 20% tensile strain.

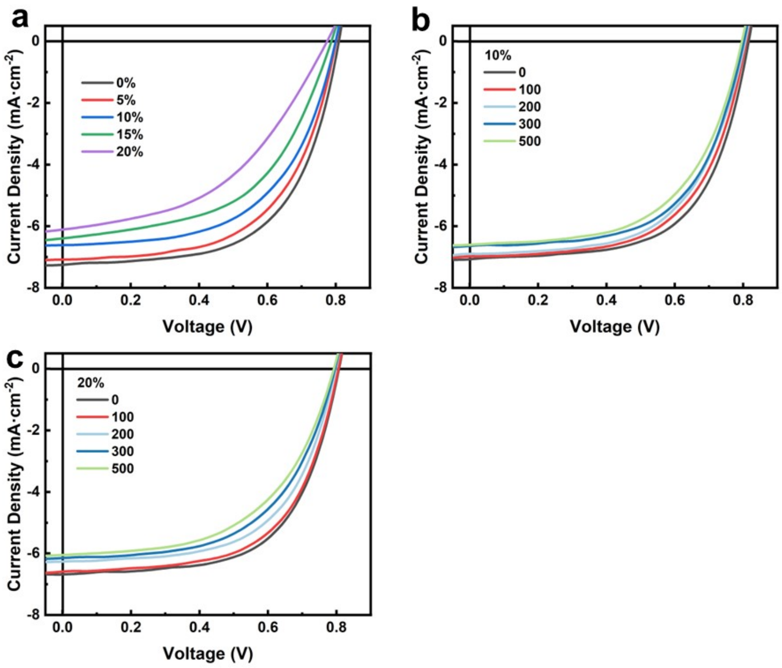

Figure S30 The representative *J-V* curves of the devices based on PBDB-T:N2200 a) under different tensile strains, b) after continuous stretch-release cycles with 10% tensile strain, c) after continuous stretch-release cycles with 20% tensile strain.

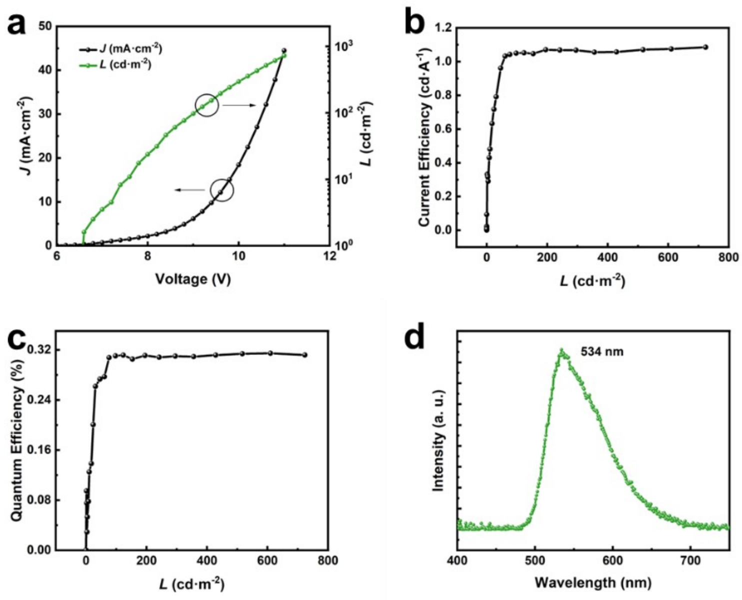

Figure S31 a) Current density and luminance - voltage curves, b) current efficiency - luminance curve, c) quantum efficiency – luminance curve, d) emission spectra of the *is*-OLED device.

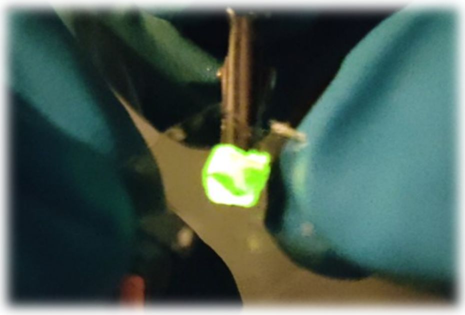

Figure S32 Photograph of the OLED device at an external bias of 9V under tensile strain by a probe poking

Table S1 Parameters of the devices based on AZO with different thickness*.

AZO thickness	V_{OC} (V)	J_{SC} (mA·cm^{-2})	FF	PCE (%)
25	0.844 (0.838±0.008)	26.06 (25.83±0.23)	0.765 (0.759±0.004)	16.83 (16.42±0.22)
30	0.843 (0.837±0.008)	26.01 (25.57±0.28)	0.763 (0.760±0.004)	16.73 (16.27±0.26)
40	0.838 (0.831±0.010)	25.84 (25.18±0.41)	0.743 (0.739±0.003)	16.09 (15.46±0.32)
60	0.829 (0.820±0.007)	25.17 (24.54±0.39)	0.727 (0.722±0.004)	15.17 (14.53±0.29)
80	0.822 (0.817±0.006)	24.76 (23.91±0.36)	0.709 (0.702±0.004)	14.43 (13.72±0.31)

*The average values and the standard deviation were obtained from ten independent cells.

Table S2 Parameters of devices based on AgNWs back electrode with different concentrations*.

AgNWs concentration	V_{OC} **(V)**	J_{SC} **(mA·cm^{-2})**	**FF**	**PCE (%)**
2	0.761 (0.742±0.012)	15.08 (14.96±0.46)	0.326 (0.303±0.019)	3.74 (3.36±0.21)
2.5	0.774(0.761±0.015)	15.71 (15.31±0.56)	0.375 (0.335±0.025)	4.56 (3.90±0.28)
3.3	0.787(0.776±0.010)	17.96 (17.37±0.40)	0.440 (0.403±0.029)	6.22 (5.43±0.51)
5	0.811(0.795±0.015)	18.51 (17.92±0.43)	0.497 (0.447±0.031)	7.46 (6.37±0.57)
6.7	0.813(0.799±0.012)	18.72 (18.13±0.50)	0.527 (0.509±0.031)	8.02 (7.37±0.02)
10	0.830 (0.816±0.012)	19.20 (18.89±0.40)	0.603 (0.591±0.015)	9.61 (9.11±0.29)
10×2	0.824(0.822±0.010)	19.34 (19.07±0.36)	0.596 (0.579±0.025)	9.50 (9.08±0.39)

*The average values and the standard deviation were obtained from ten independent cells.

Table S3 Parameters of the devices based on AAA back electrode with different AZO coverage concentrations (AgNWs with 5 mg/ml)*.

AZO (wt. %)	V_{OC} (V)	J_{SC} (mA·cm^{-2})	FF	PCE (%)
2.5	0.834 (0.835±0.002)	20.87 (20.23±0.45)	0.737 (0.722±0.014)	12.83 (12.12±0.32)
1.67	0.837 (0.834±0.004)	20.63 (20.13±0.52)	0.730 (0.720±0.017)	12.61 (12.07±0.35)
0.83	0.832 (0.829±0.006)	19.74 (19.19±0.46)	0.663 (0.666±0.016)	10.89 (10.59±0.32)
0.5	0.812 (0.814±0.003)	19.04 (19.10±0.28)	0.615 (0.594±0.019)	9.55 (9.25±0.29)
0	0.813 (0.808±0.004)	17.82 (16.68±0.63)	0.497 (0.490±0.020)	7.20 (6.61±0.28)

*The average values and the standard deviation were obtained from ten independent cells.

Table S4 Parameters of the devices based on TPU@AgNWs with different AgNWs properties*.

T_{avg} (%)**	R_{sh} (Ω/sq)	V_{OC} (V)	J_{SC} (mA·cm^{-2})	FF	PCE (%)
88.2	68.1	0.817 (0.812±0.007)	25.17 (24.93±0.32)	0.703 (0.688±0.027)	14.46 (14.02±0.35)
83.1	27.3	0.831 (0.824±0.004)	25.83 (25.26±0.41)	0.739 (0.718±0.019)	15.86 (15.19±0.47)
70.7	15.8	0.834 (0.827±0.003)	21.85 (22.19±0.48)	0.743 (0.725±0.021)	13.54 (13.16±0.33)

*The device structure is TPU@AgNWs/PEDOT:PSS/PM6:BTP-eC9:PFNBr/Ag.

*The average values and the standard deviation were obtained from ten independent cells.

**Average optical transmittance between 300-1000 nm.

Table S5 Parameters of the devices based on PM6:BTP-eC9 after 200 cycles of continuous bending with different curvature radii.

Curvature radius (mm)	V_{OC} **(V)**	J_{SC} **(mA·cm^{-2})**	**FF (%)**	**PCE (%)**
20	0.811	20.13	65.86	10.75
10	0.811	20.15	66.16	10.81
6	0.811	19.69	66.15	10.57
5	0.809	19.55	65.89	10.43
2.5	0.808	19.44	65.72	10.33
0.75	0.807	19.04	65.37	10.04
Folding	0.786	17.81	58.79	8.23

Table S6 Parameters of the devices based on PM6:BTP-eC9 after continuous bending cycles with a 1.5 mm radius.

Bending cycles	V_{OC} (V)	J_{SC} (mA·cm^{-2})	FF (%)	PCE (%)
0	0.811	20.37	65.87	10.88
200	0.810	20.65	65.79	11.01
400	0.809	20.30	66.07	10.85
600	0.809	20.21	66.10	10.80
800	0.808	20.04	65.94	10.68
1000	0.809	19.69	65.82	10.48
1500	0.808	19.70	65.46	10.41
2000	0.806	19.17	65.58	10.13
3000	0.805	18.90	65.21	9.92

Table S7 Parameters of the devices based on different active layers under different tensile strain.

Active layers	Tensile strain (%)	V_{OC} (V)	J_{SC} (mA·cm^{-2})	FF (%)	PCE (%)
PM6:BTP-eC9	0	0.805	19.59	65.86	10.38
	5	0.800	18.33	64.51	9.46
	10	0.797	16.25	58.14	7.53
	15	0.791	13.52	48.06	5.14
	20	0.766	10.79	38.60	3.19
PM6:PY-IT	0	0.909	16.13	61.90	9.08
	5	0.905	15.37	60.20	8.37
	10	0.898	12.68	58.38	6.64
	15	0.884	10.58	53.52	5.01
	20	0.828	7.83	43.90	2.84
PBDB-T:N2200	0	0.808	7.28	59.67	3.51
	5	0.800	7.08	58.01	3.29
	10	0.799	6.70	55.67	2.98
	15	0.787	6.42	52.45	2.65
	20	0.775	6.33	44.23	2.17

Table S8 Parameters of the devices based on different active layers after continuous cycles of 10% tensile strain.

Active layers	**Cycles**	V_{OC} **(V)**	J_{SC} **(mA·cm^{-2})**	**FF (%)**	**PCE (%)**
PM6:BTP-eC9	0	0.807	20.13	65.53	10.65
	100	0.801	19.19	63.17	9.71
	200	0.796	18.91	62.66	9.43
	300	0.778	18.76	61.92	9.04
	500	0.780	18.28	58.17	8.29
PM6:BTP-eC9	0	0.908	16.52	61.85	9.28
	100	0.895	15.59	60.92	8.50
	200	0.87	15.26	60.32	8.01
	300	0.853	15.15	58.21	7.52
	500	0.843	14.97	57.40	7.25
PBDB-T:N2200	0	0.816	7.07	61.78	3.56
	100	0.809	6.98	60.18	3.40
	200	0.806	6.88	59.30	3.29
	300	0.798	6.63	59.87	3.17
	500	0.796	6.62	58.22	3.07

Table S9 Parameters of the devices based on different active layers after continuous cycles of 20% tensile strain.

Active layers	Cycles	**V_{OC} (V)**	**J_{SC} (mA·cm^{-2})**	**FF (%)**	**PCE (%)**
PM6:BTP-eC9	0	0.810	20.16	64.80	10.58
	100	0.784	18.81	60.21	8.88
	200	0.764	18.53	55.02	7.79
	300	0.737	17.29	46.57	5.94
	500	0.659	14.35	36.13	3.42
PM6:BTP-eC9	0	0.907	16.73	59.50	9.03
	100	0.874	16.18	53.12	7.51
	200	0.854	15.77	50.34	6.78
	300	0.842	15.46	45.59	5.93
	500	0.782	10.86	37.00	3.14
PBDB-T: N2200	0	0.807	6.82	61.81	3.40
	100	0.805	6.59	59.02	3.13
	200	0.797	6.26	59.31	2.96
	300	0.796	6.14	57.40	2.81
	500	0.792	6.05	54.92	2.63

Appendix S1 Summary of previous work about solution processed top electrode (ITO as bottom electrode)

Year	Top electrode	Device configuration	Device area (cm^2)	PCE (%)	Reference
2021	AgNWs	Glass/ITO/PEDOT:PSS/PM6:Y6/PDINO/Ag NWs	0.0314	12.1	5
2021	AgNWs	Glass/ITO/ZnO/ PBDTTT-EFT:PCBM/*s*-MoO3/AgNWs	-	4.19	6
2021	AgNWs	Glass/ITO/PEDOT:PSS/PTB7-Th:IEICO-4F/AzO/ /AgNWs	0.2	8.8	7
2019	PH1000/AI4083/EG	Glass/ITO/ZnO/P3HT:PCBM/ PH1000/AI4083/EG	0.04	2.04	8
2021	AgNPs/HMO (Opaque)	Glass/ITO/PEDOT:PSS/PM6:Y6/ZnO/AgNPs/HMO	-	15	9
2021	AgCNTs	Glass/ITO/ZnO/J71:Y6:PC71CM/MoO3/ AgCNTs	-	9.54	10
2021	PH1000	Glass/ITO/PMA-Im-PTB7-Th:IEICO-4F/PH1000	0.04	10.37	11
2020	AgNWs	Glass/ITO/ZnO/PM6:Y6/PEDOT:PSS/ AgNWs	-	9.12	12
2020	AgNWs-20	Glass/ITO/ZnO/PBDB-T-2Cl:IT-4F/MoO3/ AgNWs		6.44	13
2020	AgNPs	Glass/ITO/PEDOT:PSS/PBDB-T:IT-M/ZnO/Zr(acac)4/ AgNPs	-	9.73	14
2019	Ag paste (Opaque)	Glass/ITO/ZnO/SMD2:ITIC-Th/Bilayer HTLs/Ag paste	0.04	8.0	15
2018	PH1000	Glass/ITO/ZnO/FTAZ:IT-M/MoO3/PEDOT:PSS	0.025	5.54	16
2018	AgNWs	Glass/ITO/ZnO/PTB7-Th:PC71BM/PMA/PEDOT:PSS/AgNWs	-	5.01	17
2018	PH1000	Glass/ITO/ZnO/ PBTZT-stat-BDTT8:PCBM/ PEDOT:PSS	0.3	2.9	18
			4	2.44	18
2017	PH1000	Glass/ITO/PEIE/PTB7:PC71BM/PEDOT:PSS/PDMS	0.045	3.75	19
2016	AgNWs	Glass/ITO/PEDOT:PSS/BDTT-S-TR:PCBM/ZnO/ PDINO/AgNWs	-	3.62	20
2015	PH1000:PEG-TmDD	Glass/ITO/PEI/P3HT:ICBA/ PH1000:PEG-TmDD	-	4.1	21
2015	PH1000	Glass/LWF-PEDOT:PSS/P3HT:ICBA/HWF-PEDOT:PSS	-	4.0	22
2015	PH1000	Glass/ITO/PEI/P3HT:ICBA/PH1000/PEI/P3HT:ICBA/PEDOT-T	0.05	3.6	23
2014	PH1000	Glass/ITO/ZnO/P3HT:ICBA/PEDOT:PSS	-	4.0	24
2013	AgNWs	Glass/ITO/PBDTT-SeDPP:PC71BM/TiO2/AgNWs	-	5.5	25
		Glass/ITO/ PBDTT-FDPP-C12:PC61BM/PFN/TiO2/PEDOT/ PBDTT-SeDPP:PC71BM/TiO2/AgNWs	-	7.3	

Appendix S2 Summary of previous work about all-solution processed organic solar cells.

Year	Substrate	Device configuration	Device area (cm^2)	PCE (%)	Reference
2022	Glass (Rigid)	Glass/AgNWs/PEI-Zn/PM6:PC$_{71}$BM:Y6/PEDOT:F/AgNWs	0.041	12.83 14.62 (with mirror)	[26]
			12.2 (modulus)	15.26	
		Glass/AgNWs/PEI-Zn/ PM6:PC$_{71}$BM:BTP-eC9/PEDOT:F/AgNWs	0.041	15.26 (with mirror)	
2021	TPU (Stretchable/Opaque)	TPU/PH1000/AI4083/PM6:Y7/PNDIT-F3N-Br/EGaIn	0.0625	11.2	[27]
2021	TPU (Stretchable/Opaque)	TPU@AgNWs/PEDOT:PSS/PTB7-Th:IEICO-4F:PDMS/EGaIn	-	10.3	[28]
2021	PDMS (Stretchable/Opaque)	PDMS/PH1000/PBDB-T:PCE10:N2200/EGaIn	0.04	6.33	[29]
2020	Polyimide (Flexible)	AgNWs@PI/ZnO/PBDB-T-2F:IDIC:Y6/ HMoO3/PEDOT:PSS/AgNWs	0.04	11.9 (with mirror)	[30]
			1	10.3 (with mirror)	[30]
2020	PET (Flexible)	PH1000/AI4083/PM6:Y6/ZnO/PH1000	0.06	11.12	[31]
2018	Polyurethane (Flexible)	Ag/ZnO np/ P3HT:ICBA/ PEDOT:PSS/ AgNWs	0.03	1.71	[32]
2018	PET (Flexible)	PAMD-Ag/PEI/P3HT:PC61BM/PEDOT:PSS	-	3.03	[33]
2017	Glass (Rigid)	Ag ink/ZnO/PBTZT-stat-BDTT-8:PCBM/ PEDOT:PSS:Ag NW	1.04	4.5	[34]
			19.7 (Module)	3.6	
	PET (Flexible)		17.7 (Module)	2.9	
2016	PES (Flexible)	PEDOT:PSS/PEIE/P3HT:IDT-2BR/ PEDOT:PSS	0.043	2.88	[35]
2016	PET (Flexible)	Ag gird/PEDOT:PSS/ZnO/ PffBT4T2OD:PC61BM:PC71BM/PEDOT:PSS:AgNWs	0.1	6.6	[36]
			1	5.8	[36]
2016	Glass (Rigid)	AgNWs/ZnO/PV2000:PC70BM/ PEDOT:PSS/AgNWs	1	4.3	[37]
2016	Glass (Rigid)	PEDOT:PSS/PEI/P3HT:ICBA /PEDOT:PSS	-	4.0	[22]

2016	PET (Flexible)	Ag gird/PEDOT:PSS/ZnO/ PTB7-TH:IEIC/PEDOT:PSS/Ag gird	0.95-1.05	1.79	38
2016	Glass (Rigid)	PEDOT:PSS/PEIE/TQ1:PC71BM/PEDOT:PSS	0.04	2.54	39
2016	PET (Flexible)	Ag gird/PEDOT:PSS/ZnO/ P3HT:ICBA/PEDOT:PSS/Ag grid	57	2	40
2016	PES (Flexible)	(PEDOT:PSS/PEI/P3HT:ICBA)*5/PEDOT:PSS (6-junction)	-	6.5	41
2016	PET (Flexible)	AgNWs/ZnO/P3HT:PCBM/PEDOT:PSS/ZnO/Polymer Generation 2.1:PCBM/PEDOT:PSS/Ag gird	0.8-1	2.66	42
2016	IF Fabric (Flexible)	AgNWs/ZnO np/ P3HT:ICBA/PEDOT:PSS/AgNWs	0.06	0.14	43
2015	PET (Flexible)	Ag gird/PEDOT:PSS/ZnO/ P3HT:F(DPP)2B2/PEDOT:PSS/Ag grid	1	0.65	44
2015	PES (Flexible)	PEDOT:PSS/PEI/P3HT:ICBA/ PEDOT:PSS	-	3.3	45
2015	PET (Flexible)	Ag gird/PEDOT:PSS/ZnO/ PBDTTT-C-:DCIDT2T/PEDOT:PSS/Ag gird	1	1.019	46
2015	Glass (Rigid)	Glass/P_Ag/pDPP5T-2/AgNWs	0.15	4.74	47
		Ag/PEDOT:PSS/GEN-3:PCBM/ZnO/ N-PEDOT/pDPP5T2:PCBM /ZnO/AgNWs (2-junction)	0.15	5.81	
2015	Glass (Rigid)	Ag gird/PEDOT:PSS/ZnO/ P3HT:PCBM/PEDOT:PSS/Ag	1	4.1	48
2015	PET (Flexible)	Ag grid/PEDOT:PSS/ZnO np/PBDTTTz4:PCBM/PEDOT:PSS/ZnO np/PDTPI:PCBM/PEDOT:PSS/Ag grid	0.8	1.72	49
2015	Glass (Rigid)	PEDOT:PSS/PEI/P3HT:ICBA/PEDOT:PSS	-	3.8	50
2015	Glass (Rigid)	Ag/AZO/P3HT:PCBM/PEDOT:PSS/AgNWs	0.104	2.5	51
2015	PET (Flexible)	PEDOT:PSS/PEIE/TQ-1:PCBM/PEDOT:PSS	0.1	0.4	52
2014	PET (Flexible)	Ag gird/PEDOT:PSS/ZnO np/PBDTTT-CT:PC71BM/PEDOT:PSS /Ag gird	1	2.09	53
2014	Glass (Rigid)	AgNWs/PEDOT:PSS/ DPP:PCBM/ZnO/AgNWs	0.104	2.09	54
2014	PET	Ag/PEDOT:PSS/ZnO/MH301:PCBM/PFN/PEDOT:PSS/	52.2	1.76	55

	(Flexible)	Zn O/MH306:PCBM/PFN/PEDOT:PSS/Ag grid			
2014	PET (Flexible)	Ag gird/PEDOT:PSS/ZnO/ PBDTTHDDTBTff:PCBM/PEDOT:PSS/Ag gird	1	3.8	56
2014	PET (Flexible)	Ag/ZnO np/PBDTT-FTTE:PC71BM/ PEDOT:PSS/AgNWs	0.4	4.8	57
2014	PET (Flexible)	Ag/ZnO/P3HT:PCBM/PEDOT:PSS/ZnO/ PPTBTT:PCBM/PEDOT: PSS /Ag grid	1	2.39	58
		Ag/ZnO/PBDTTT:PCBM/PEDOT:PSS/Ag gird	0.8	2.73	
2014	Glass (Rigid)	PEDOT:PSS/PCDTBT:PCBM/ZnO np/Ag ink	0.5	3.13	59
2014	Glass (Rigid)	AgNWs/TiOx/ZnO/ P3HT:PCBM/PEDOT:PSS/GO	0.24	2.3	60
2014	PET (Flexible)	Ag gird/PEDOT:PSS/ZnO/P1:PCBM/PEDOT:PSS/ZnO/P2: PCBM /PEDOT :PSS/ Ag gird	-	2.67	61
2014	PET (Flexible)	Ag gird/PEDOT:PSS/ZnO/ P3HT:PCBM/PEDOT:PSS/Ag gird	1	2.05	62
2014	PET (Flexible)	PEDOT:PSS/ZnO np/ P3HT:PCBM/PEDOT:PSS/Carbon	-	1.83	63
2014	PET (Flexible)	Ag gird/PEDOT:PSS/ZnO/ P3HTT-DPP10%:PCBM/PEDOT:PSS	1.1	1.36	64
2014	PET (Flexible)	Ag gird/PEDOT:PSS/ZnO/ SM1:PC61BM/PEDOT:PSS/Ag gird	1	1.01	65
2014	Glass (Rigid)	Graphene/PEDOT:PSS/PSEHTT:IC60BA/ZnO/PEDOT: PSS/ PBDTT-DPP:PC71BM/TiO2/AgNWs	0.04	8.02	66
2014	PET (Flexible)	Ag gird/PEDOT:PSS/ZnO/ PDTSTTz4:PCBM/PEDOT:PSS/Ag gird	1	3.2	67
2013	PET (Flexible)	Ag gird/PEDOT:PSS/ZnO/ P3HT:PCBM/PEDOT:PSS/Ag gird	142	1.82	68
2013	PET (Flexible)	Ag gird/PEDOT:PSS/ZnO/ PDTSTTz4:PCBM/PEDOT:PSS/Ag gird	1	3.5	69
2013	Glass (Rigid)	AgNWs/AZO/P3HT:PCBM:SiPCPDTBT/PEDOT:PSS/ AgNWs	0.104	2.2	70

1. Z. Zhang, W. Wang, Y. Jiang, Y. X. Wang, Y. Wu, J. C. Lai, S. Niu, C. Xu, C. C. Shih, C. Wang, H. Yan,

L. Galuska, N. Prine, H. C. Wu, D. Zhong, G. Chen, N. Matsuhisa, Y. Zheng, Z. Yu, Y. Wang, R. Dauskardt, X. Gu, J. B. Tok and Z. Bao, *Nature*, 2022, **603**, 624-630.

2. H. Hu, H. Tian, Y. Gao, Z. Wan, L. Wang, H. Xu, C. Wang, J. Shao and Z. Zheng, *Journal of the Mechanics and Physics of Solids*, 2023, **170**, 105121.
3. C. M. Stafford, C. Harrison, K. L. Beers, A. Karim, E. J. Amis, M. R. VanLandingham, H. C. Kim, W. Volksen, R. D. Miller and E. E. Simonyi, *Nat Mater*, 2004, **3**, 545-550.
4. D. Tahk, H. H. Lee and D.-Y. Khang, *Macromolecules*, 2009, **42**, 7079-7083.
5. H. I. Jeong, S. Biswas, S. C. Yoon, S. J. Ko, H. Kim and H. Choi, *Adv. Energy Mater.*, 2021, **11**, 2102397.
6. H.-C. Yang, W. Zha, C.-N. Weng, C.-H. Chen, H.-W. Zan, K.-W. Su, Q. Luo, C.-Q. Ma, Y.-C. Chao and H.-F. Meng, *Optical Materials*, 2021, **112**.
7. N. Chaturvedi, N. Gasparini, D. Corzo, J. Bertrandie, N. Wehbe, J. Troughton and D. Baran, *Advanced Functional Materials*, 2021, **31**.
8. D. H. Kim, D. J. Lee, B. Kim, C. Yun and M. H. Kang, *Solid-State Electronics*, 2020, **169**.
9. X. He, Y. Wang, L. Zhang, R. Zhang, J. Kim, K. S. Wong, Y. Chen and W. C. H. Choy, *Advanced Functional Materials*, 2021, **31**.
10. Y. Zhang, X. He, D. Babu, W. Li, X. Gu, C. Shan, A. K. K. Kyaw and W. C. H. Choy, *Advanced Optical Materials*, 2021, **9**.
11. L. Hu, W. You, L. Sun, S. Yu, M. Yang, H. Wang, Z. Li and Y. Zhou, *Chem Commun (Camb)*, 2021, **57**, 2689-2692.
12. Y. Xiong, R. E. Booth, T. Kim, L. Ye, Y. Liu, Q. Dong, M. Zhang, F. So, Y. Zhu, A. Amassian, B. T. O'Connor and H. Ade, *Solar RRL*, 2020, **4**, 2000328.
13. X. Sun, W. Zha, T. Lin, J. Wei, I. Ismail, Z. Wang, J. Lin, Q. Luo, C. Ding, L. Zhang, Z. Su, B. Chu, D. Zhang and C.-Q. Ma, *Journal of Materials Science*, 2020, **55**, 14893-14906.
14. X. He, Y. Wang, H. Lu, D. Ouyang, Z. Huang and W. C. H. Choy, *Journal of Materials Chemistry A*, 2020, **8**, 6083-6091.
15. Y. W. Han, S. J. Jeon, H. S. Lee, H. Park, K. S. Kim, H. W. Lee and D. K. Moon, *Advanced Energy Materials*, 2019, **9**.
16. P. Sen, Y. Xiong, Q. Zhang, S. Park, W. You, H. Ade, M. W. Kudenov and B. T. O'Connor, *ACS Appl Mater Interfaces*, 2018, **10**, 31560-31567.
17. G. Ji, Y. Wang, Q. Luo, K. Han, M. Xie, L. Zhang, N. Wu, J. Lin, S. Xiao, Y. Q. Li, L. Q. Luo and C. Q. Ma, *ACS Appl Mater Interfaces*, 2018, **10**, 943-954.
18. Y.-C. Huang, C.-W. Chou, D.-H. Lu, C.-Y. Chen and C.-S. Tsao, *IEEE Journal of Photovoltaics*, 2018, **8**, 144-150.
19. X. Fan, B. Xu, N. Wang, J. Wang, S. Liu, H. Wang and F. Yan, *Adv. Electron. Mater*, 2017, **3**, 1600471.
20. J. Min, C. Bronnbauer, Z.-G. Zhang, C. Cui, Y. N. Luponosov, I. Ata, P. Schweizer, T. Przybilla, F. Guo, T. Ameri, K. Forberich, E. Spiecker, P. Bäuerle, S. A. Ponomarenko, Y. Li and C. J. Brabec,

Advanced Functional Materials, 2016, **26**, 4543-4550.

21. Z. Li, W. Meng, J. Tong, C. Zhao, F. Qin, F. Jiang, S. Xiong, S. Zeng, L. Xu, B. Hu and Y. Zhou, *Solar Energy Materials and Solar Cells*, 2015, **137**, 311-318.
22. Z. Li, Y. Liang, Z. Zhong, J. Qian, G. Liang, K. Zhao, H. Shi, S. Zhong, Y. Yin and W. Tian, *Synthetic Metals*, 2015, **210**, 363-366.
23. J. Tong, S. Xiong, Z. Li, F. Jiang, L. Mao, W. Meng and Y. Zhou, *Applied Physics Letters*, 2015, **106**.
24. L. Yin, Z. Zhao, F. Jiang, Z. Li, S. Xiong and Y. Zhou, *Organic Electronics*, 2014, **15**, 2593-2598.
25. C.-C. Chen, L. Dou, J. Gao, W.-H. Chang, G. Li and Y. Yang, *Energy & Environmental Science*, 2013, **6**.
26. Y. Jiang, X. Dong, L. Sun, T. Liu, F. Qin, C. Xie, P. Jiang, L. Hu, X. Lu, X. Zhou, W. Meng, N. Li, C. J. Brabec and Y. Zhou, *Nature Energy*, 2022, **7**, 352-359.
27. J. Noh, G.-U. Kim, S. Han, S. J. Oh, Y. Jeon, D. Jeong, S. W. Kim, T.-S. Kim, B. J. Kim and J.-Y. Lee, *ACS Energy Lett.*, 2021, **6**, 2512-2518.
28. Z. Wang, M. Xu, Z. Li, Y. Gao, L. Yang, D. Zhang and M. Shao, *Adv. Funct. Mater.*, 2021, **31**, 2103534.
29. Q. Zhu, J. Xue, L. Zhang, J. Wen, B. Lin, H. B. Naveed, Z. Bi, J. Xin, H. Zhao, C. Zhao, K. Zhou, S. Frank Liu and W. Ma, *Small*, 2021, **17**, 2007011.
30. L. Sun, W. Zeng, C. Xie, L. Hu, X. Dong, F. Qin, W. Wang, T. Liu, X. Jiang, Y. Jiang and Y. Zhou, *Adv. Mater.*, 2020, **32**, 1907840.
31. X. Fan, R. Wen, Y. Xia, J. Wang, X. Liu, H. Huang, Y. Li, W. Zhu, Y. Cheng, L. Ma, J. Fang, H. Tsai and W. Nie, *Solar RRL*, 2020, **4**.
32. S. Arumugam, Y. Li, M. Glanc-Gostkiewicz, R. N. Torah and S. P. Beeby, *IEEE Journal of Photovoltaics*, 2018, **8**, 1710-1715.
33. H. Zhen, K. Li, Y. Zhang, L. Chen, L. Niu, X. Wei, X. Fang, P. You, Z. Liu, D. Wang, F. Yan and Z. Zheng, *Journal of Semiconductors*, 2018, **39**.
34. M. Koppitz, N. Hesse, D. Landerer, L. Graf von Reventlow, E. Wegner, J. Czolk and A. Colsmann, *Energy Technology*, 2017, **5**, 1105-1111.
35. Y. Wang, B. Jia, F. Qin, Y. Wu, W. Meng, S. Dai, Y. Zhou and X. Zhan, *Polymer*, 2016, **107**, 108-112.
36. J. Czolk, D. Landerer, M. Koppitz, D. Nass and A. Colsmann, *Advanced Materials Technologies*, 2016, **1**.
37. P. Maisch, K. C. Tam, L. Lucera, H.-J. Egelhaaf, H. Scheiber, E. Maier and C. J. Brabec, *Organic Electronics*, 2016, **38**, 139-143.
38. K. Liu, T. T. Larsen-Olsen, Y. Lin, M. Beliatis, E. Bundgaard, M. Jørgensen, F. C. Krebs and X. Zhan, *Journal of Materials Chemistry A*, 2016, **4**, 1044-1051.
39. Z. Tang, A. Elfwing, A. Melianas, J. Bergqvist, Q. Bao and O. Inganäs, *Journal of Materials Chemistry A*, 2015, **3**, 24289-24296.
40. R. Garcia-Valverde, J. A. Villarejo, M. Hösel, M. V. Madsen, R. R. Søndergaard, M. Jørgensen and

F. C. Krebs, *Solar Energy Materials and Solar Cells*, 2016, **144**, 48-54.
41. J. Tong, S. Xiong, Y. Zhou, L. Mao, X. Min, Z. Li, F. Jiang, W. Meng, F. Qin, T. Liu, R. Ge, C. Fuentes-Hernandez, B. Kippelen and Y. Zhou, *Materials Horizons*, 2016, **3**, 452-459.
42. D. Angmo, T. R. Andersen, J. J. Bentzen, M. Helgesen, R. R. Søndergaard, M. Jørgensen, J. E. Carlé, E. Bundgaard and F. C. Krebs, *Advanced Functional Materials*, 2015, **25**, 4539-4547.
43. S. Arumugam, Y. Li, S. Senthilarasu, R. Torah, A. L. Kanibolotsky, A. R. Inigo, P. J. Skabara and S. P. Beeby, *Journal of Materials Chemistry A*, 2016, **4**, 5561-5568.
44. W. Liu, H. Shi, T. R. Andersen, N. K. Zawacka, P. Cheng, E. Bundgaard, M. Shi, X. Zhan, F. C. Krebs and H. Chen, *RSC Advances*, 2015, **5**, 36001-36006.
45. W. Meng, R. Ge, Z. Li, J. Tong, T. Liu, Q. Zhao, S. Xiong, F. Jiang, L. Mao and Y. Zhou, *ACS Appl Mater Interfaces*, 2015, **7**, 14089-14094.
46. P. Cheng, H. Bai, N. K. Zawacka, T. R. Andersen, W. Liu, E. Bundgaard, M. Jorgensen, H. Chen, F. C. Krebs and X. Zhan, *Adv Sci (Weinh)*, 2015, **2**, 1500096.
47. F. Guo, N. Li, V. V. Radmilović, V. R. Radmilović, M. Turbiez, E. Spiecker, K. Forberich and C. J. Brabec, *Energy & Environmental Science*, 2015, **8**, 1690-1697.
48. T. M. Eggenhuisen, Y. Galagan, A. F. K. V. Biezemans, T. M. W. L. Slaats, W. P. Voorthuijzen, S. Kommeren, S. Shanmugam, J. P. Teunissen, A. Hadipour, W. J. H. Verhees, S. C. Veenstra, M. J. J. Coenen, J. Gilot, R. Andriessen and W. A. Groen, *Journal of Materials Chemistry A*, 2015, **3**, 7255-7262.
49. R. G. Brandt, W. Yue, T. R. Andersen, T. T. Larsen-Olsen, M. Hinge, E. Bundgaard, F. C. Krebs and D. Yu, *Journal of Materials Chemistry C*, 2015, **3**, 1633-1639.
50. Z. Li, F. Qin, T. Liu, R. Ge, W. Meng, J. Tong, S. Xiong and Y. Zhou, *Organic Electronics*, 2015, **21**, 144-148.
51. J. Krantz, K. Forberich, P. Kubis, F. Machui, J. Min, T. Stubhan and C. J. Brabec, *Organic Electronics*, 2015, **17**, 334-339.
52. L. M. Andersson, *Energy Technology*, 2015, **3**, 437-442.
53. P. Cheng, Y. Lin, N. K. Zawacka, T. R. Andersen, W. Liu, E. Bundgaard, M. Jørgensen, H. Chen, F. C. Krebs and X. Zhan, *J. Mater. Chem. A*, 2014, **2**, 19542-19549.
54. F. Guo, P. Kubis, T. Stubhan, N. Li, D. Baran, T. Przybilla, E. Spiecker, K. Forberich and C. J. Brabec, *ACS Appl Mater Interfaces*, 2014, **6**, 18251-18257.
55. T. R. Andersen, H. F. Dam, M. Hösel, M. Helgesen, J. E. Carlé, T. T. Larsen-Olsen, S. A. Gevorgyan, J. W. Andreasen, J. Adams, N. Li, F. Machui, G. D. Spyropoulos, T. Ameri, N. Lemaître, M. Legros, A. Scheel, D. Gaiser, K. Kreul, S. Berny, O. R. Lozman, S. Nordman, M. Välimäki, M. Vilkman, R. R. Søndergaard, M. Jørgensen, C. J. Brabec and F. C. Krebs, *Energy & Environmental Science*, 2014, **7**.
56. J. E. Carlé, M. Helgesen, N. K. Zawacka, M. V. Madsen, E. Bundgaard and F. C. Krebs, *Journal of Polymer Science Part B: Polymer Physics*, 2014, **52**, 893-899.
57. F. Nickel, T. Haas, E. Wegner, D. Bahro, S. Salehin, O. Kraft, P. A. Gruber and A. Colsmann, *Solar*

Energy Materials and Solar Cells, 2014, **130**, 317-321.

58. D. Angmo, H. F. Dam, T. R. Andersen, N. K. Zawacka, M. V. Madsen, J. Stubager, F. Livi, R. Gupta, M. Helgesen, J. E. Carlé, T. T. Larsen-Olsen, G. U. Kulkarni, E. Bundgaard and F. C. Krebs, *Energy Technology*, 2014, **2**, 651-659.
59. S. Jung, A. Sou, K. Banger, D.-H. Ko, P. C. Y. Chow, C. R. McNeill and H. Sirringhaus, *Advanced Energy Materials*, 2014, **4**.
60. J. H. Yim, S. Y. Joe, C. Pang, K. M. Lee, H. Jeong, J. Y. Park, Y. H. Ahn, J. C. de Mello and S. Lee, *ACS Nano*, 2014, **8**, 2857-2863.
61. H. F. Dam, T. R. Andersen, E. B. L. Pedersen, K. T. S. Thydén, M. Helgesen, J. E. Carlé, P. S. Jørgensen, J. Reinhardt, R. R. Søndergaard, M. Jørgensen, E. Bundgaard, F. C. Krebs and J. W. Andreasen, *Advanced Energy Materials*, 2015, **5**.
62. N. K. Zawacka, T. R. Andersen, J. W. Andreasen, L. H. Rossander, H. F. Dam, M. Jørgensen and F. C. Krebs, *J. Mater. Chem. A*, 2014, **2**, 18644-18654.
63. G. A. dos Reis Benatto, B. Roth, M. V. Madsen, M. Hösel, R. R. Søndergaard, M. Jørgensen and F. C. Krebs, *Advanced Energy Materials*, 2014, **4**.
64. T. R. Andersen, H. F. Dam, B. Burkhart, D. Angmo, M. Corazza, B. C. Thompson and F. C. Krebs, *J. Mater. Chem. C*, 2014, **2**, 9412-9415.
65. W. Liu, S. Liu, N. K. Zawacka, T. R. Andersen, P. Cheng, L. Fu, M. Chen, W. Fu, E. Bundgaard, M. Jørgensen, X. Zhan, F. C. Krebs and H. Chen, *J. Mater. Chem. A*, 2014, **2**, 19809-19814.
66. A. R. b. M. Yusoff, S. J. Lee, F. K. Shneider, W. J. da Silva and J. Jang, *Advanced Energy Materials*, 2014, **4**.
67. J. E. Carlé, M. Helgesen, M. V. Madsen, E. Bundgaard and F. C. Krebs, *J. Mater. Chem. C*, 2014, **2**, 1290-1297.
68. F. C. Krebs, M. Hösel, M. Corazza, B. Roth, M. V. Madsen, S. A. Gevorgyan, R. R. Søndergaard, D. Karg and M. Jørgensen, *Energy Technology*, 2013, **1**, 378-381.
69. M. Helgesen, J. E. Carlé and F. C. Krebs, *Advanced Energy Materials*, 2013, **3**, 1664-1669.
70. F. Guo, X. Zhu, K. Forberich, J. Krantz, T. Stubhan, M. Salinas, M. Halik, S. Spallek, B. Butz, E. Spiecker, T. Ameri, N. Li, P. Kubis, D. M. Guldi, G. J. Matt and C. J. Brabec, *Advanced Energy Materials*, 2013, **3**, 1062-1067.